INTERNATIONAL JOURNAL FOR NUMERICAL METHODS IN FLUIDS
Int. J. Numer. Meth. Fluids 2004; **44**:645–663 (DOI: 10.1002/fld.665)

A Lagrangian Discontinuous Galerkin-type method on unstructured meshes to solve hydrodynamics problems

R. Loubère[1,†], J. Ovadia[2,‡] and R. Abgrall[3,§]

[1]*Los Alamos National Laboratory, T-7, Mathematical Modeling and Analysis Group, MS B284, Los Alamos, New Mexico 87545, U.S.A.*
[2]*CEA-CESTA, BP No2, 33114 Le Barp, France*
[3]*Institut Universitaire de France, Université Bordeaux 1, MAB Mathématiques Appliquées de Bordeaux, 351 Cours de la Libération, 33650 Talence Cedex, France*

SUMMARY

This paper concerns a new Lagrangian Discontinuous Galerkin-type method to solve 2D fluid flows on unstructured meshes. By using a basis of Bernstein polynomials of degree m in each triangle, we define a diffusion process which ensures positivity and stability of the scheme. The discontinuities of the physical variables at the interfaces between cells are solved with an acoustic Riemann solver. A remeshing/remapping process is performed with a particle method: the remapping is locally conservative and its accuracy can be adapted to the accuracy of the numerical method. Copyright © 2004 John Wiley & Sons, Ltd.

KEY WORDS: Lagrangian method; Discontinuous Galerkin method; remapping; hydrodynamics problem; isentropic compression

1. INTRODUCTION

In this paper, a new Lagrangian Discontinuous Galerkin-type method in 2D is developed. This method is devoted to multidimensional hydrodynamics problems on unstructured meshes in Lagrangian coordinates. A non-classical formulation of the Euler equations in Lagrangian coordinates is used. The main principles of the Discontinuous Galerkin method are adapted to this Lagrangian formulation. If the movement is highly disturbed the method may require a remeshing/remapping process. A particle method has been developed to remap the domain.

*Correspondence to: R. Loubère, MS B284, Los Alamos National Laboratory T7, Los Alamos, NM, 87544, U.S.A.
†loubere@lanl.gov
‡jean.ovadia@cea.fr
§abgrall@math.u-bordeaux.fr

Contract/grant sponsor: The financial support of the first author was a "CEA-Region Aquitaine" PhD grant as he was PhD student at the university of Bordeaux, France and at the CEA-CESTA, Le Barp, France

Received 2 January 2003
Revised 23 September 2003

This remapping is locally conservative and its accuracy can be adapted to the accuracy of the numerical method.

The paper is organized as follow. Section 2 gives an overview of the Lagrangian system of conservation laws. The hierarchical numerical method is presented in Section 3 of this paper. Section 4 presents the locally conservative remeshing/remapping process made with a particle method. An algorithm of the method is given in Section 5. Finally Section 6 presents several numerical test cases in 1D and 2D.

2. 2D LAGRANGIAN SYSTEM OF CONSERVATION LAWS

Let $(\xi,\eta)^t$ be the 2D Lagrangian coordinates and $(X((\xi,\eta),t),Y((\xi,\eta),t))^t$ the Eulerian ones. They are linked to each other by the transformation ($(u,v)^t$ is the fluid velocity)

$$X((\xi,\eta),t=0)=\xi, \quad Y((\xi,\eta),t=0)=\eta \tag{1}$$

$$\frac{\partial}{\partial t}X=u, \quad \frac{\partial}{\partial t}Y=v \tag{2}$$

The Jacobian matrix describes the time evolution of these two systems of coordinates. The Jacobian is the determinant of this matrix and can be associated with a local compression/expansion rate. This Jacobian may not change sign during time evolution in order to define a bijection between Lagrangian and Eulerian coordinates

$$\mathscr{J}=\begin{pmatrix}\partial_\xi X & \partial_\xi Y\\ \partial_\eta X & \partial_\eta Y\end{pmatrix} \quad \begin{cases}J((\xi,\eta),t)=\partial_\xi X\partial_\eta Y-\partial_\xi Y\partial_\eta X\\ J((\xi,\eta),0)=1\end{cases} \tag{3}$$

The 2D Lagrangian system of conservation laws can be written as (see Reference [1])

$$\frac{\partial}{\partial t}J-\vec{\nabla}_\xi.(u(\overrightarrow{\nabla_\xi Y})_\perp-v(\overrightarrow{\nabla_\xi X})_\perp)=0 \tag{4}$$

$$\frac{\partial}{\partial t}(\rho J)=0 \tag{5}$$

$$\frac{\partial}{\partial t}(\rho uJ)+\vec{\nabla}_\xi.(p(\overrightarrow{\nabla_\xi Y})_\perp)=0 \tag{6}$$

$$\frac{\partial}{\partial t}(\rho vJ)+\vec{\nabla}_\xi.(-p(\overrightarrow{\nabla_\xi X})_\perp)=0 \tag{7}$$

$$\frac{\partial}{\partial t}(\rho eJ)+\vec{\nabla}_\xi.(pu(\overrightarrow{\nabla_\xi Y})_\perp-pv(\overrightarrow{\nabla_\xi X})_\perp)=0 \tag{8}$$

$$p=(\gamma-1)\rho(e-\tfrac{1}{2}(u^2+v^2)) \tag{9}$$

We use the notation

$$(\overrightarrow{\nabla_\xi A})_\perp = \begin{pmatrix} -\partial_\eta A \\ \partial_\xi A \end{pmatrix}$$

for all scalar A. Equation (9) can be replaced with any other equation of state. A more concise notation of the previous system leads to a *physical system of conservation laws*

$$\frac{\partial}{\partial t}(UJ) + \overrightarrow{\nabla_\xi}.\overrightarrow{\varphi}_\perp = 0 \tag{10}$$

$$U = (\rho, \rho u, \rho v, \rho e, 1)^{\mathrm{t}} \tag{11}$$

$$\overrightarrow{F}(U) = \begin{pmatrix} F_1 \\ F_2 \end{pmatrix} = \left(\begin{pmatrix} 0 \\ 0 \end{pmatrix}, \begin{pmatrix} p \\ 0 \end{pmatrix}, \begin{pmatrix} 0 \\ p \end{pmatrix}, p \begin{pmatrix} u \\ v \end{pmatrix}, - \begin{pmatrix} u \\ v \end{pmatrix} \right) \tag{12}$$

$$\overrightarrow{\varphi}_\perp = F_1(\overrightarrow{\nabla_\xi Y})_\perp - F_2(\overrightarrow{\nabla_\xi X})_\perp \tag{13}$$

and to a *geometrical system of conservation laws*

$$\frac{\partial}{\partial t}\overrightarrow{\nabla_\xi X} - \overrightarrow{\nabla_\xi u} = 0, \quad \frac{\partial}{\partial t}\overrightarrow{\nabla_\xi Y} - \overrightarrow{\nabla_\xi v} = 0 \tag{14}$$

In References [2, 3] hyperbolicity studies of the above systems can be found. Both systems are hyperbolic but their union (called complete system) is only weakly hyperbolic: even if all the eigenvalues are real, there is no complete basis of eigenvectors. However, if the numerical method does not have to determine a complete basis of eigenvectors then this system can be considered to be hyperbolic.

3. THE HIERARCHICAL NUMERICAL SCHEMES—A LAGRANGIAN DISCONTINUOUS GALERKIN APPROACH

Let $\Omega = \bigcup_{c=1}^{N_T} T_c$, with $T_c \equiv T$ being the triangle under consideration, be a non-structured mesh. The nodes of T are locally labelled 1,2,3, the side h in front of the node number i ($i = 1, 2, 3$) is side number i and the normal unit output vector to h is called $\overrightarrow{v}_h$, the boundary of T is ∂T and $\overset{\circ}{T} = T/\partial T$. T_h is the neighbourhood triangle having h as a common side.

In every triangle T one can define a Bernstein basis of polynomials of degree m: $\{\sigma_k\}_{k=1}^{B_m}$. If $\lambda_1, \lambda_2, \lambda_3 = 1 - \lambda_1 - \lambda_2$ are the barycentric coordinates in T then the Bernstein basis of polynomials are the monomials of the development

$$(\lambda_1 + \lambda_2 + \lambda_3)^m \equiv 1 \tag{15}$$

For example if $m = 1$ the basis consists of 3 Bernstein polynomials

$$\sigma_1 = \lambda_1, \quad \sigma_2 = \lambda_2, \quad \sigma_3 = \lambda_3 \tag{16}$$

For $m = 2$ the basis is made up of 6 Bernstein polynomials

$$\sigma_1 = \lambda_1^2, \quad \sigma_2 = 2\lambda_1\lambda_2, \quad \sigma_3 = \lambda_2^2, \quad \sigma_4 = 2\lambda_2\lambda_3, \quad \sigma_5 = \lambda_3^2, \quad \sigma_6 = 2\lambda_1\lambda_3 \tag{17}$$

The number of Bernstein's polynomials of degree m is equal to B_m (see Reference [3] for details).

Every component of Equation (10) is multiplied with every σ_k to give the moment equations.

$$\int_\Omega \left(\frac{\partial}{\partial t}(UJ) + \{\overrightarrow{\nabla}_\xi . \overrightarrow{\varphi}_\perp\} \right) \sigma_k \, \mathrm{d}\xi \, \mathrm{d}\eta = 0 \tag{18}$$

These $\{\bullet\}$ mean that $\bullet$ has to be considered in the sense of a distribution. The Discontinuous Galerkin principles imply that the functions are polynomials in each cell, such that on a triangle T the divergence of $\overrightarrow{\varphi}_\perp$ is split into two parts:

$$\{\overrightarrow{\nabla}_\xi . \overrightarrow{\varphi}_\perp\} \equiv \begin{cases} \overrightarrow{\nabla}_\xi . \overrightarrow{\varphi}_\perp & \text{if } \overrightarrow{\xi} \in \overset{\circ}{T} \\ [\overrightarrow{\varphi}_\perp|_{T_h} - \overrightarrow{\varphi}_\perp|_T] . \overrightarrow{v}_h & \text{if } \overrightarrow{\xi} \in h \end{cases} \tag{19}$$

Equation (18) is equivalent to ($T_c \equiv T$)

$$\sum_{c=1}^{M} \left\{ \int_T \frac{\partial}{\partial t}(UJ)\sigma_k \, \mathrm{d}\xi \, \mathrm{d}\eta + \int_{\overset{\circ}{T}} \overrightarrow{\nabla}_\xi . \overrightarrow{\varphi}_\perp \sigma_k \, \mathrm{d}\xi \, \mathrm{d}\eta \right.$$
$$\left. + \sum_{h \in \partial T} \int_h [\overrightarrow{\varphi}_\perp|_{T_h} . \overrightarrow{v}_h - \overrightarrow{\varphi}_\perp|_T . \overrightarrow{v}_h] \sigma_k \, \mathrm{d}\mu \right\} = 0 \tag{20}$$

The discontinuity on h is split into two contributions by using the intermediate value $\overline{\int_h \overrightarrow{\varphi}_\perp \sigma_k \, \mathrm{d}\mu}^*$

$$\int_h [\overrightarrow{\varphi}_\perp|_{T_h} - \overrightarrow{\varphi}_\perp|_T] \sigma_k \, \mathrm{d}\mu = \underbrace{\left[\int_h \overrightarrow{\varphi}_\perp|_{T_h} \sigma_k \, \mathrm{d}\mu - \overline{\int_h \overrightarrow{\varphi}_\perp \sigma_k \, \mathrm{d}\mu}^* \right]}_{\text{contribution for } T_h}$$
$$+ \underbrace{\left[\overline{\int_h \overrightarrow{\varphi}_\perp \sigma_k \, \mathrm{d}\mu}^* - \int_h \overrightarrow{\varphi}_\perp|_T \sigma_k \, \mathrm{d}\mu \right]}_{\text{contribution for } T}$$

Whatever the intermediate value conservation will be respected. The same process is repeated on each side h such that the moment equations are finally given by

$$\int_T \frac{\partial}{\partial t}(UJ)\sigma_k \, \mathrm{d}\xi \, \mathrm{d}\eta + \int_{\overset{\circ}{T}} \overrightarrow{\nabla}_\xi . \overrightarrow{\varphi}_\perp \sigma_k \, \mathrm{d}\xi \, \mathrm{d}\eta$$
$$+ \sum_{h \in \partial T} \left[\overline{\int_h \overrightarrow{\varphi}_\perp . \overrightarrow{v}_h \sigma_k \, \mathrm{d}\mu}^* - \int_h \overrightarrow{\varphi}_\perp|_T . \overrightarrow{v}_h \sigma_k \, \mathrm{d}\mu \right] = 0 \tag{21}$$

A Green formula for the second term yields

$$\int_T \frac{\partial}{\partial t}(UJ)\sigma_k \,\mathrm{d}\xi\,\mathrm{d}\eta - \int_{\overset{\circ}{T}} \overrightarrow{\varphi}_\perp.\overrightarrow{\nabla_\xi \sigma_k}\,\mathrm{d}\xi\,\mathrm{d}\eta + \sum_{h\in\partial T} \overline{\int_h \overrightarrow{\varphi}_\perp.\overrightarrow{v}_h \sigma_k \,\mathrm{d}\mu}^{*} = 0 \tag{22}$$

If we define $M_{UJ,k} := \int_T (UJ)\sigma_k \,\mathrm{d}\xi\,\mathrm{d}\eta$ to be the moment of UJ, $M_{\nabla\varphi,k} := \int_{\overset{\circ}{T}} \overrightarrow{\nabla}_\xi.\overrightarrow{\varphi}_\perp \sigma_k \,\mathrm{d}\xi\,\mathrm{d}\eta$ to be the interior cell term,

$$\sum_{h\in\partial T}\left[M^*_{\varphi,k,h} - M_{\varphi,k,h}\right] := \sum_{h\in\partial T}\left[\overline{\int_h \overrightarrow{\varphi}_\perp.\overrightarrow{v}_h \sigma_k \,\mathrm{d}\mu}^{*} - \int_h \overrightarrow{\varphi}_\perp|_T.\overrightarrow{v}_h \sigma_k \,\mathrm{d}\mu\right]$$

to be the border terms, then system (21) becomes

$$\frac{\partial}{\partial t} M_{UJ,k} + M_{\nabla\varphi,k} + \sum_{h\in\partial T}[M^*_{\varphi,k,h} - M_{\varphi,k,h}] = 0 \tag{23}$$

Let $[t_n, t_{n+1}] \subset [0,T]$ with $T>0$ and $\Delta t = t_{n+1} - t_n$, then the time discretization is given as

$$\frac{\partial}{\partial t}(M_{UJ,k}) \simeq \frac{M^{n+1}_{UJ,k} - M_{UJ,k}}{\Delta t} \tag{24}$$

superscript $n+1$ is the variable at time $t = t_{n+1}$ and the absence of a superscript implies that the variable has to be taken at time $t = t_n$. Equation (23) becomes

$$M^{n+1}_{UJ,k} = M_{UJ,k} - \Delta t M_{\nabla\varphi,k} - \Delta t \sum_{h\in\partial T}[M^*_{\varphi,k,h} - M_{\varphi,k,h}] \tag{25}$$

Interior cell terms approximation: For all $k = 1,\ldots,B_m$

$$M_{\nabla\varphi,k} = \int_{\overset{\circ}{T}} \overrightarrow{\nabla}_\xi.\overrightarrow{\varphi}_\perp \sigma_k \,\mathrm{d}\xi\,\mathrm{d}\eta \quad \text{with } \overrightarrow{\varphi}_\perp = F_1(\overrightarrow{\nabla_\xi Y})_\perp - F_2(\overrightarrow{\nabla_\xi X})_\perp \tag{26}$$

Suppose that $\overrightarrow{\varphi}_\perp$ is a vector whose components are polynomials of degree m, then

$$\overrightarrow{\varphi}_\perp(\overrightarrow{\xi}) = \sum_{i=1}^{B_m} \overrightarrow{\varphi}_{\perp,i}\sigma_i(\overrightarrow{\xi}) \Rightarrow M_{\nabla\varphi,k} = \sum_{i=1}^{B_m} \overrightarrow{\varphi}_{\perp,i}.\int_{\overset{\circ}{T}} \overrightarrow{\nabla_\xi \sigma_i}\sigma_k \,\mathrm{d}\xi\,\mathrm{d}\eta \tag{27}$$

with $\overrightarrow{\varphi}_{\perp,i}$ the i-component in the Bernstein basis. To determine (27) we have to compute $\overrightarrow{\varphi}_{\perp,i}$ for all i. As moments of UJ are known at $t = t_n$, we can define

$$\hat{U}(\overrightarrow{\xi}) = \sum_{i=1}^{B_m} \hat{U}_i \sigma_i(\overrightarrow{\xi}) \quad \text{with } \hat{U}_i = \left(\frac{M_{UJ,i}}{M_{J,i}}\right) \tag{28}$$

then an approximation of $\overrightarrow{F}(U)$ is given by

$$\overrightarrow{F}(U)(\overrightarrow{\xi}) \simeq \overrightarrow{F}(\hat{U})(\overrightarrow{\xi}) = \sum_{i=1}^{B_m} \overrightarrow{\hat{F}_i}\,\sigma_i(\overrightarrow{\xi}) \quad \text{with } \overrightarrow{\hat{F}_i} = \overrightarrow{F}(\hat{U}_i) \tag{29}$$

If we suppose that $\overrightarrow{\nabla_\xi X}$ and $\overrightarrow{\nabla_\xi Y}$ are polynomials then

$$\overrightarrow{\nabla_\xi X} \simeq \overrightarrow{\widehat{\nabla_\xi X}}(\overrightarrow{\xi}) = \sum_{i=1}^{B_m} \overrightarrow{\widehat{\nabla_\xi X}_i}\sigma_i(\overrightarrow{\xi}) \tag{30}$$

$$\overrightarrow{\nabla_\xi Y} \simeq \overrightarrow{\widehat{\nabla_\xi Y}}(\overrightarrow{\xi}) = \sum_{i=1}^{B_m} \overrightarrow{\widehat{\nabla_\xi Y}_i}\sigma_i(\overrightarrow{\xi}) \tag{31}$$

A $\mathbb{P}_m$ approximation of $\overrightarrow{\varphi}_\perp$ is then computed as an (m)-diffusive Bernstein polynomial

$$\overrightarrow{\varphi}_\perp \simeq \sum_{i=1}^{B_m} \overrightarrow{\hat{\varphi}}_{\perp,i}\sigma_i(\xi) \quad \text{with } \overrightarrow{\hat{\varphi}}_{\perp,i} = \left(\hat{F}_{1,i}(\overrightarrow{\widehat{\nabla_\xi Y}})_{\perp,i} - \hat{F}_{2,i}(\overrightarrow{\widehat{\nabla_\xi X}})_{\perp,i}\right) \tag{32}$$

Remark 1
The definition of an (m)-diffusive Bernstein polynomial of a function $A \in L^1(T)$ is

$$\forall (x,y)^t \in T \quad \hat{A}(x,y) = \sum_{i=1}^{B_m} \left(\frac{\int_T A(\xi,\eta)\sigma_i(\xi,\eta)\,\mathrm{d}\xi\,\mathrm{d}\eta}{\int_T \sigma_i(\xi,\eta)\,\mathrm{d}\xi\,\mathrm{d}\eta}\right)\sigma_i(x,y) \tag{33}$$

In Reference [3] some properties of such polynomials are shown.¶ By using (m)-diffusive polynomials numerical diffusion is added to the scheme and the stability is increased. Moreover, (m)-diffusive polynomials ensure that the Jacobian, density and pressure polynomials remain positive if and only if all Bernstein components are positive.

Interior cell terms are computed as

$$M_{\nabla\varphi,k} \simeq \sum_{j=1}^{B_m} \overrightarrow{\hat{\varphi}}_{\perp,j}.\int_{\overset{\circ}{T}} \overrightarrow{\nabla_\xi \sigma_j}\sigma_k\,\mathrm{d}\xi\,\mathrm{d}\eta \tag{34}$$

Approximation of the border terms: The border terms are split into two parts

$$\sum_{h\in\partial T}[M^*_{\varphi,k,h} - M_{\varphi,k,h}] = \sum_{h\in\partial T}\left[\overline{\int_h \overrightarrow{\varphi}_\perp.\overrightarrow{v}_h\sigma_k\,\mathrm{d}\mu}^{\,*} - \int_h \overrightarrow{\varphi}_\perp|_T.\overrightarrow{v}_h\sigma_k\,\mathrm{d}\mu\right] \tag{35}$$

An approximation of $\overrightarrow{\varphi}_\perp$ has already been given therefore

$$\int_h \overrightarrow{\varphi}_\perp|_T.\overrightarrow{v}_h\sigma_k\,\mathrm{d}\mu \simeq \sum_{j=1}^{B_m}\overrightarrow{\hat{\varphi}}_{\perp,j}.\overrightarrow{v}_h\int_h \sigma_i\sigma_k\,\mathrm{d}\mu \tag{36}$$

The star term is the solution of the moment Riemann problem on the side h in the direction $\overrightarrow{n}_h.\overrightarrow{n}_h$ is the outgoing normal vector to ∂K the image of ∂T in the transformation from Lagrangian coordinates to Eulerian ones. The physical moments on both sides of h are given by

$$\int_{\partial K} U(S)\sigma_k(S)\,\mathrm{d}S = \int_{\partial T} U\sigma_k\sqrt{((\overrightarrow{\nabla_\xi Y})_\perp.\overrightarrow{v}_{\partial T})^2 + (-(\overrightarrow{\nabla_\xi X})_\perp.\overrightarrow{v}_{\partial T})^2}\,\mathrm{d}\mu \tag{37}$$

¶(i) $\int_T \hat{A}\,\mathrm{d}\xi\,\mathrm{d}\eta = \int_T A\,\mathrm{d}\xi\,\mathrm{d}\eta$, (ii) $A>0 \Rightarrow \hat{A}>0$, (iii) $\|\hat{A}-A\|_p \overset{m\to\infty}{\to} 0$ for all $1 \leqslant p < \infty$.

The approximation of (37) uses (m)-diffusive polynomials

$$\widehat{UG}(\mu) := \sum_{i=1}^{B_m} \widehat{UG}_i \sigma_i(\mu) \quad \widehat{UG}_i = \hat{U}_i \sqrt{((\overrightarrow{\widehat{\nabla_\xi Y}})_{\perp,i}.\overrightarrow{v}_{\partial T})^2 + (-(\overrightarrow{\widehat{\nabla_\xi X}})_{\perp,i}.\overrightarrow{v}_{\partial T})^2} \tag{38}$$

$$(\overrightarrow{\widehat{\nabla_\xi X}})_{\perp,i} \quad \text{and} \quad (\overrightarrow{\widehat{\nabla_\xi Y}})_{\perp,i}$$

are given due to (30) and (31) (see (51) and (52)).

Moment Riemann problem: The physical states on both sides of h are given by

$$\widehat{\widehat{U}}^T_{h,k} := \frac{\sum_{i=1}^{B_m} \widehat{UG}_i \int_{h\in\partial T} \sigma_i\sigma_k \,\mathrm{d}\mu}{\sum_{i=1}^{B_m} \hat{G}_i \int_{h\in\partial T} \sigma_i\sigma_k \,\mathrm{d}\mu} \quad UG, G \text{ defined in } T \tag{39}$$

$$\widehat{\widehat{U}}^{T_h}_{h,k} := \frac{\sum_{i=1}^{B_m} \widehat{UG}_i \int_{h\in\partial T_h} \sigma_i\sigma_k \,\mathrm{d}\mu}{\sum_{i=1}^{B_m} \widehat{UG}_i \int_{h\in\partial T_h} \sigma_i\sigma_k \,\mathrm{d}\mu} \quad UG, G \text{ defined in } T_h \tag{40}$$

Using (39) and (40) two densities $(\rho^T_{h,k}, \rho^{T_h}_{h,k})$, two pressures $(p^T_{h,k}, p^{T_h}_{h,k})$, two sound velocities $(c^T_{h,k}, c^{T_h}_{h,k})$ and two velocities $(v^T_{h,k}, v^{T_h}_{h,k})$ can be computed for each Bernstein basis σ_k on the side h. The Riemann problem on these two states is solved with the following acoustic Riemann solver:

$$\begin{aligned} \overset{*}{v}_{h,k} &= \frac{p^{T_h}_{h,k} - p^T_{h,k} + (\rho c v)^T_{h,k} + (\rho c v)^{T_h}_{h,k}}{(\rho c)^T_{h,k} + (\rho c)^{T_h}_{h,k}} \\ RP(\widehat{\widehat{U}}^T_{h,k}, \widehat{\widehat{U}}^{T_h}_{h,k}, \overrightarrow{n}_{\partial K}) &\nearrow \\ &\searrow \\ \overset{*}{p}_{h,k} &= p^T_{h,k} - (\rho c)^T_{h,k}(\overset{*}{v}_{h,k} - v^T_{h,k}) \end{aligned} \tag{41}$$

The increments of each variable are then defined as

$$U = \rho u : M^*_{\varphi,k,h} = \overset{*}{p}_{h,k} \int_{h\in\partial T} \overrightarrow{\widehat{\nabla_\xi Y}}_\perp . \overrightarrow{v}_h \sigma_k \,\mathrm{d}\mu \tag{42}$$

$$U = \rho v : M^*_{\varphi,k,h} = \overset{*}{p}_{h,k} \int_{h\in\partial T} -\overrightarrow{\widehat{\nabla_\xi X}}_\perp . \overrightarrow{v}_h \sigma_k \,\mathrm{d}\mu \tag{43}$$

$$U = \rho e : M^*_{\varphi,k,h} = \overset{*}{p}_{h,k} \overset{*}{v}_{h,k} \int_{h\in\partial T} \hat{G}\sigma_k \,\mathrm{d}\mu \tag{44}$$

$$U = 1 : M^*_{\varphi,k,h} = \overset{*}{v}_{h,k} \int_{h\in\partial T} \hat{G}\sigma_k \,\mathrm{d}\mu \tag{45}$$

The explicit scheme can now be written as

$$M_{UJ,k}^{n+1} = M_{UJ,k} - \Delta t \sum_{j=1}^{B_m} \overrightarrow{\hat{\varphi}}_{\perp,j} \cdot \int_T^{\circ} \overrightarrow{\nabla_\xi \sigma_j} \sigma_k \, \mathrm{d}\xi \, \mathrm{d}\eta$$

$$-\Delta t \sum_{h \in \partial T} \left[M_{\varphi,k,h}^{*} - \sum_{j=1}^{B_m} \overrightarrow{\hat{\varphi}}_{\perp,j} \cdot \overrightarrow{v}_h \int_h \sigma_j \sigma_k \, \mathrm{d}\mu \right] \tag{46}$$

The explicit discretization of the geometrical system yields

$$M_{\overrightarrow{\nabla_\xi X},j}^{n+1} = M_{\overrightarrow{\nabla_\xi X},j} + \Delta t \int_T \overrightarrow{\widehat{\nabla_\xi u}} \sigma_j \, \mathrm{d}\xi \, \mathrm{d}\eta \tag{47}$$

$$M_{\overrightarrow{\nabla_\xi Y},j}^{n+1} = M_{\overrightarrow{\nabla_\xi Y},j} + \Delta t \int_T \overrightarrow{\widehat{\nabla_\xi v}} \sigma_j \, \mathrm{d}\xi \, \mathrm{d}\eta \tag{48}$$

such that

$$M_{\overrightarrow{\nabla_\xi X},j}^{n+1} = M_{\overrightarrow{\nabla_\xi X},j} + \Delta t \sum_{k=1}^{B_m} \hat{u}_k \int_T \overrightarrow{\nabla_\xi \sigma_k} \sigma_j \, \mathrm{d}\xi \, \mathrm{d}\eta \tag{49}$$

$$M_{\overrightarrow{\nabla_\xi Y},j}^{n+1} = M_{\overrightarrow{\nabla_\xi Y},j} + \Delta t \sum_{k=1}^{B_m} \hat{v}_k \int_T \overrightarrow{\nabla_\xi \sigma_k} \sigma_j \, \mathrm{d}\xi \, \mathrm{d}\eta \tag{50}$$

As

$$\overrightarrow{\widehat{\nabla_\xi X_j}} = \frac{\int_T \overrightarrow{\nabla_\xi X} \sigma_j \, \mathrm{d}\xi \, \mathrm{d}\eta}{\int_T \sigma_j \, \mathrm{d}\xi \, \mathrm{d}\eta} = \frac{M_{\overrightarrow{\nabla_\xi X},j}}{\int_T \sigma_j \, \mathrm{d}\xi \, \mathrm{d}\eta}$$

and

$$\overrightarrow{\widehat{\nabla_\xi Y_j}} = \frac{\int_T \overrightarrow{\nabla_\xi Y} \sigma_j \, \mathrm{d}\xi \, \mathrm{d}\eta}{\int_T \sigma_j \, \mathrm{d}\xi \, \mathrm{d}\eta} = \frac{M_{\overrightarrow{\nabla_\xi Y},j}}{\int_T \sigma_j \, \mathrm{d}\xi \, \mathrm{d}\eta}$$

then the gradients of X and Y are given by

$$\overrightarrow{\widehat{\nabla_\xi X_j}}^{n+1} = \overrightarrow{\widehat{\nabla_\xi X_j}} + \Delta t \sum_{k=1}^{B_m} \hat{u}_k \frac{\int_T \overrightarrow{\nabla_\xi \sigma_k} \sigma_j \, \mathrm{d}\xi \, \mathrm{d}\eta}{\int_T \sigma_j \, \mathrm{d}\xi \, \mathrm{d}\eta} \tag{51}$$

$$\overrightarrow{\widehat{\nabla_\xi Y_j}}^{n+1} = \overrightarrow{\widehat{\nabla_\xi Y_j}} + \Delta t \sum_{k=1}^{B_m} \hat{v}_k \frac{\int_T \overrightarrow{\nabla_\xi \sigma_k} \sigma_j \, \mathrm{d}\xi \, \mathrm{d}\eta}{\int_T \sigma_j \, \mathrm{d}\xi \, \mathrm{d}\eta} \tag{52}$$

Step size: Δt is limited by two conditions: a Lagrangian CFL-type condition and a Jacobian condition. Because the Jacobian has to remain positive we enforce Δt the value to be such that $M_{J,k}^{n+1}$ will remain positive for all k (as will be the polynomials $\hat{J}$ and $\hat{\rho}$). A Runge–Kutta (RK) method has been used to increase the value of Δt.

Slope type limiting: The use of (m)-diffusive polynomials adds some numerical diffusion to the method in such a way that the positivity (of Jacobian and density polynomials) is ensured

and the scheme is stable without any slope type limiting for $m \leqslant 2$, aside from strong shock waves. In the general case a slope-type limiter is added, its philosophy is: '*if the compression is maximum in T* (*with respect to its three neighbours*), *then all variables UJ are replaced by their* (*m*)*-diffusive polynomial*'.

Boundary conditions are simulated by prescribing the pressure $\overset{*}{p}_{h,k}$ or the normal velocity $\overset{*}{v}_{h,k}$, on the side in contact with the external world.

4. REMAPPING/REMESHING PROCESS—A PARTICLE METHOD

Lagrangian methods are known to be accurate because the mesh is refined near the compression area and unrefined near the expansion area. However, one of the drawbacks of Lagrangian methods is the fact that for highly disturbed flows, positivity of the Jacobian cannot be guaranteed. The previous numerical method ensures Jacobian positivity by reducing Δt. But if Δt tends to 0 the solution is to remap/remesh the domain.

The remapping/remeshing process is a critical phase in a Lagrangian hydrodynamics code because it can destroy all the efforts made by the scheme to be conservative and accurate. The point is to build a remapping process (i) locally conservative, (ii) with the same accuracy as the scheme.

If $f \in \mathbb{P}_m(\Omega)$, the accuracy of the remeshing/remapping process is measured as its capability to give a polynomial approximation of f called $\tilde{f} \in \mathbb{P}_m(\Omega)$ such that $\tilde{f} = f$ after several remapping phases.

4.1. Projection on particles

Definition 1

A particle is a Dirac function $\delta_{\overrightarrow{\xi}_p}(\overrightarrow{\xi})$ located in $\overrightarrow{\xi}_p$ carrying six weights

$$(\omega U)_p = (\omega\rho, \omega\rho u, \omega\rho v, \omega\rho e, \omega)_p, \quad U_p = \frac{(\omega U)_p}{\omega_p}$$

A particle p belongs to T if $\overrightarrow{\xi}_p \in T$. So we can define discrete moments with respect to the Bernstein basis.

Definition 2

Discrete moments of degree (m) are the (B_m)-vectors (vector of size B_m)

$$(M_{\omega_\cdot}) \equiv \begin{pmatrix} M_{\omega U,1} \\ M_{\omega U,2} \\ \vdots \\ M_{\omega U,B_m} \end{pmatrix} = \begin{pmatrix} \sum_{p\in T} \omega_p U_p \sigma_1^{(n)}(\xi_p) \\ \sum_{p\in T} \omega_p U_p \sigma_2^{(n)}(\xi_p) \\ \vdots \\ \sum_{p\in T} \omega_p U_p \sigma_{B_m}^{(n)}(\xi_p) \end{pmatrix}$$

Lemma 1
Let $N \geqslant B_m$ be distinct points in T called $\vec{\xi}_p$, $p = 1, \ldots, N$. Let $(M_{UJ,.})$ be the m moments given by the numerical scheme. If the weights $(\omega U)_p$ (associated to the position $\vec{\xi}_p$) are located on a polynomial of degree m, then a unique population of N particles exists such that for all $k = 1, \ldots, B_m$

$$M_{\omega U,k} = M_{UJ,k} \tag{53}$$

Proof
See Reference [3]. □

Point (i) is now fullfilled because Equation (53) implies that all the information carried by the moments has been projected on particle weights; no hypothesis has been made on the position of the particles. Then any polynomial of degree less than m is exactly integrated with this method if the mesh does not change (for example to plot the results).

4.2. Projection from particles

In the case, if we want to remesh/remap the domain we have to define a more accurate numerical integration. Indeed if the N particles are located at the Gauss points $\vec{\xi}_g$ with Gauss weights w_g then the numerical integration

$$M_{UJ,k} := \int_T (UJ)(\vec{\xi})\sigma_k(\vec{\xi})\,\mathrm{d}\xi\,\mathrm{d}\eta = \sum_{g=1}^{N} w_g (UJ)(\vec{\xi}_g)\sigma_k(\vec{\xi}_g) \tag{54}$$

is exact if $N \geqslant B_m$ in T. The same idea as Gauss quadrature is used but we will not enforce the particle positions.

Let us choose a new mesh. Let the current triangle in the new mesh be τ. Bernstein polynomials have changed in the new cells but the positions of the particles and their weights $(UJ)(\vec{\xi}_p)$ have not changed. Suppose there are $\mathcal{N}$ particles in τ ($\mathcal{N}$ can be different from N). Then we have the lemma

Lemma 2
Let $\vec{\xi}_g$, $g = 1, \ldots, \mathcal{N}$ be $\mathcal{N}$ distinct points in τ, then the quadrature problem

$$\mathcal{M}_{UJ,k} := \int_\tau (UJ)(\vec{\xi})\sigma_k(\vec{\xi})\,\mathrm{d}\xi\,\mathrm{d}\eta \equiv \sum_{g=1}^{\mathcal{N}} \mathcal{W}_g (UJ)(\vec{\xi}_g)\sigma_k(\vec{\xi}_g) \tag{55}$$

for all $k = 1, \ldots, B_m$ and for all polynomial $(UJ) \in \mathbb{P}_m(\Omega)$ has a unique solution if

$$\text{(i) } \mathcal{N} \geqslant B_{m+1}; \quad \text{(ii) } \forall g = 1, 2, \ldots \mathcal{N}, \quad \mathcal{W}_g = \tilde{\mathcal{W}}(\vec{\xi}_g) \text{ with } \tilde{\mathcal{W}} \in \mathbb{P}_{2m}(\tau)$$

Proof
See Reference [3]. □

If enough particles are in each triangle τ then the numerical integration of any polynomial of degree m is exact. Therefore the numerical diffusion due to the remapping process is very low and the accuracy of the remapping can be adapted to the accuracy of the scheme.

The moments in triangle τ give an initialization on the new mesh for the numerical method

$$\forall 1 \leqslant k \leqslant B_m, \quad \mathscr{M}_{UJ,k} := \sum_{q=1}^{\mathscr{N}} \mathscr{W}_q (UJ)_q \sigma_k(\xi_q, \eta_q) \tag{56}$$

4.3. *Eulerian particle position*

The Lagrangian particle position $(\xi_p, \eta_p)^t \in T$ is by definition fixed in time. The Eulerian position $(X_p, Y_p)^t$ changes with the velocity defined in T (recall $\widehat{UJ} \in \mathbb{P}_m(T)$)

$$\hat{u}_p^{n+1} = \frac{\widehat{\rho u J}^{n+1}(\xi_p, \eta_p)}{\widehat{\rho J}^{n+1}(\xi_p, \eta_p)} \tag{57}$$

$$\hat{v}_p^{n+1} = \frac{\widehat{\rho v J}^{n+1}(\xi_p, \eta_p)}{\widehat{\rho J}^{n+1}(\xi_p, \eta_p)} \tag{58}$$

then ($(\Delta t)_k$ it is the kth timestep value)

$$X_p^{n+1} = \xi_p + \sum_{k=1}^{n+1} (\Delta t)_k \hat{u}_p^k \tag{59}$$

$$Y_p^{n+1} = \eta_p + \sum_{k=1}^{n+1} (\Delta t)_k \hat{v}_p^k \tag{60}$$

In this paper, we did not present the way to choose a new mesh (remeshing process). Actually due to the remapping method, whatever the new mesh, if it respects the requirements of the lemmas then the remapping will be valid and accurate.

Note that after several Lagrangian steps, the Lagrangian mesh is almost impossible to be expressed in Eulerian coordinates: a node has as many velocities as neighbour cells, the velocity along an edge is a polynomial so that a straight line can turn into a curve (if $m \geqslant 2$). But we do not need this expression. As all the computations, the remeshing/remapping method is expressed in Lagrangian coordinates. Only the visualization of the results is performed in Eulerian coordinates, thanks to the particle method.

5. ALGORITHM

Let us present a sketch of the algorithm.

Initial data:

Moments $M_{UJ,j}, \overrightarrow{\widehat{\nabla_\xi X}}_j, \overrightarrow{\widehat{\nabla_\xi Y}}_j$ for all Bernstein polynomial σ_j at time t_n

Lagrangian scheme
Interior cell terms (27):

Use of (m)-diffusive polynomials $\hat{U}, \widehat{\overrightarrow{\nabla_\xi X}}, \widehat{\overrightarrow{\nabla_\xi Y}}$ to get (27)

Border terms (32):

On edge h between triangles T and T_h

(i) define the moments along the current edge with (38)

(ii) use the moment Riemann problem (41) to split the discontinuity into two contributions for T and T_h

Time step Δt:

Must fulfill the Jacobian positivity (and eventually the pressure positivity) and the CFL type condition.

Time Incrementation:

Explicit/Runge–Kutta time discretization to compute moments of

(i) physical variables $M_{UJ,j}^{n+1}$,

(ii) geometrical variables $\widehat{\overrightarrow{\nabla_\xi X}}_j^{n+1}, \widehat{\overrightarrow{\nabla_\xi Y}}_j^{n+1}$

End of the Lagrangian scheme

Limitation.

If a limitation criterium is true for a triangle,
Then all variables UJ are replaced by their (m)-diffusive polynomials.

Remeshing/Remapping.

If a remeshing/remapping criterium is true,
Then use the particle method.

6. NUMERICAL TESTS

The present method can be written for any m, with a different time discretization (explicit, RK, implicit), with or without slope type limiting on unstructured meshes and has been tested in 1D and 2D on several classical test cases, see References [3, 4] for details of the test cases.

All the tests have been performed with $m = 2$ and a 2-step Runge–Kutta time discretization. No remeshing/remapping was necessary even if a strong compression has been observed (see Reference [3] for the validation of the remeshing/remapping process).

For the 1D test cases, the initial states are given in Table I and a comparison with Eulerian schemes has been added. These Eulerian schemes are labelled as follows: CFLF (composite scheme), PPM (piecewise parabolic method of Woodward and Collela), WENO5 (weighted non-oscillatory 5th-order scheme), CWENO3 (3rd-order conservative weighted non-oscillatory scheme). More Eulerian results can be found in the review article [4] of R. Liska and B. Wendroff. For the 1D test cases the results are the average value in the middle of the cell. The first test case called *123 problem* has been chosen to test the behaviour of the method on simple rarefaction waves, the *Sod shock tube* to see if the method is able to handle a shock wave and a contact discontinuity, the *blastwave* to test the method in the presence of interacting shock waves and contact discontinuities.

123 problem in 1D: Two strong rarefaction waves are initiated in the middle of the domain [0,1] and they are moving towards the boundaries. The resulting middle state is close to vacuum for density and pressure. The difficulty of this test is to reproduce the right internal

Table I. Initial data of the 123 problem, the blastwave problem, the Sod tube problem.

123	Left	Right
ρ	1	1
u	-2	2
p	0.4	0.4

Blast	Left	Mid.	Right
ρ	1	1	1
u	0	0	0
p	1000	0.01	100

Sod	Left	Right
ρ	1	0.125
u	0	0
p	1	0.1

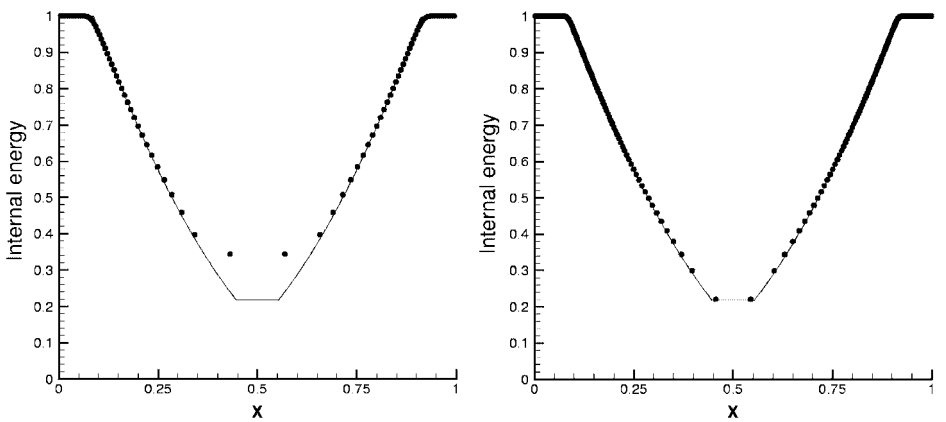

Figure 1. 123 problem—Internal energy given by the 1D method for $m = 2$ with 100 cells (left) and 250 cells (right) vs. exact solution.

energy which is not close to zero. The initial density is equal to 1, the initial pressure is 0.4 and the velocity is $u_L = -2$, $u_R = 2$ with the discontinuity located at $x = 0.5$, $\gamma = 1.4$.

The internal energy for 100 and 250 cells is presented in Figure 1 for the present method at time $t = 0.15$ with the exact solution in a straight line. In Figure 2 the results obtained with the classical Eulerian schemes for 100 cells are presented. It seems that most of the Eulerian schemes are not able to compute the internal energy very well (see Reference [4]). With the present method the internal energy is better resolved especially with 250 cells.

Sod shock tube in 1D: This classical Riemann problem generates simple waves (rarefaction, contact and shock) separated by constant states. Two initial gases ($\rho_L = 1.0$, $u_L = 0.0$, $p_L = 1.0$

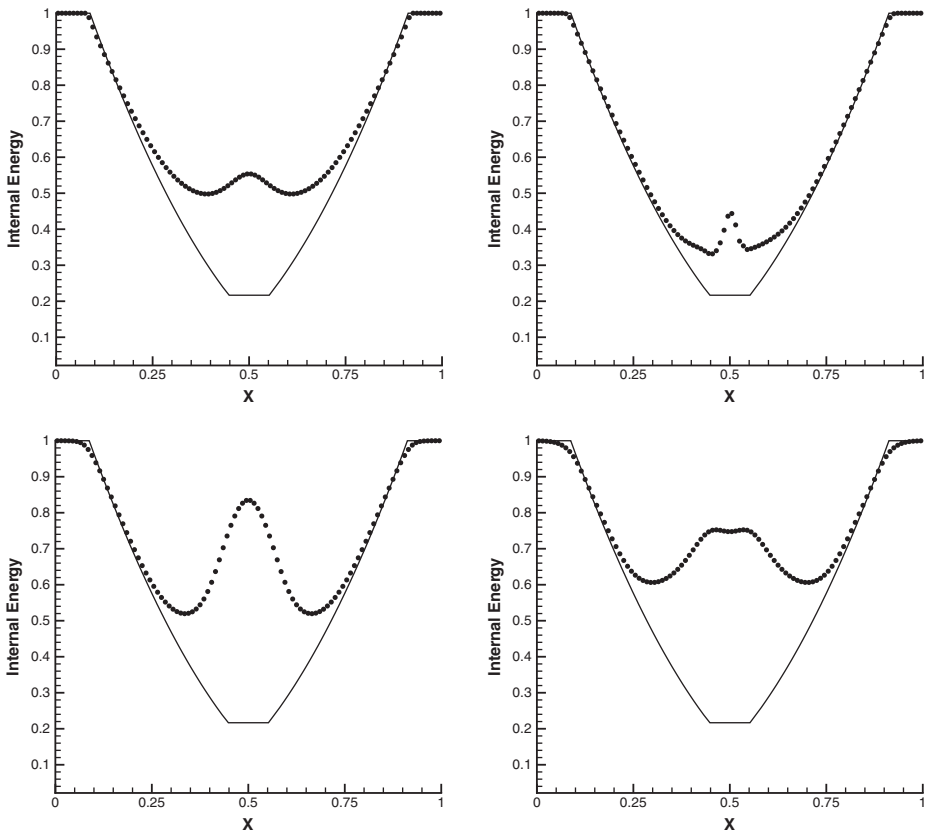

Figure 2. 123 problem—Internal energy given by Eulerian methods with 100 cells vs. exact solution.

and $\rho_R = 0.125$, $u_R = 0.0$, $p_R = 0.1$ and $\gamma = 1.4$) are splitting the domain [0,1] into two equal parts. The rarefaction wave is moving to the left whereas the contact and the shock wave are moving with a positive velocity.

The density and pressure are presented in Figure 3 for the present method (200 cells) with the exact solution in a straight line at time $t = 0.153$. Even if the limiter is neither a classical slope-type limiter used in Eulerian methods, nor a classical artificial viscosity term used in Lagrangian methods, it seems that this limiter is enough to stabilize the scheme. Moreover, the undershoot at the contact discontinuity seems to be a classical behaviour of most of the Lagrangian schemes.

Blastwave in 1D: This classical test case has been proposed by Collela and Woodward to compute the interaction of waves from two Riemann problems with reflecting boundary conditions. The interval is $x \in [0,1]$, the initial discontinuities are located at $x_1 = 0.1$ and $x_2 = 0.9$. The initial density is 1 everywhere, the gas has a zero velocity and $\gamma = 1.4$. Two pressure discontinuities ($p_l = 1000$, $p_m = 0.01$, $p_r = 100$) are generating complex interactions between shock waves, rarefaction waves and contact discontinuities. The final time of the simulation is $t = 0.038$.

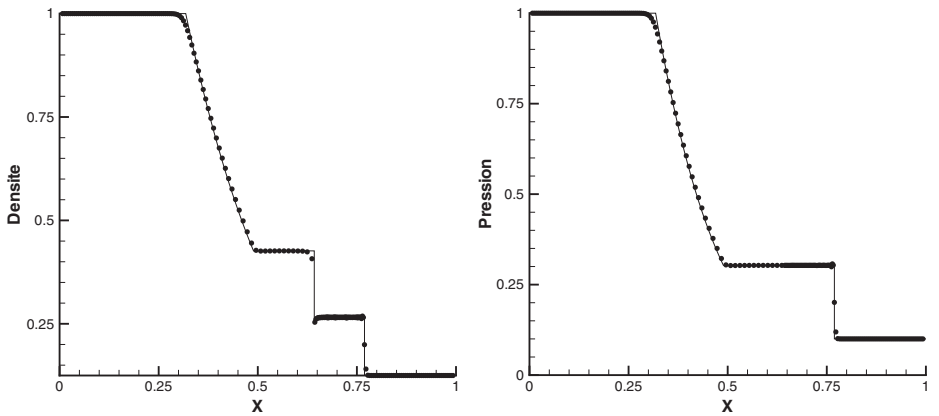

Figure 3. Sod tube—Density and pressure given by the 1D method for $m = 2$ with 200 cells.

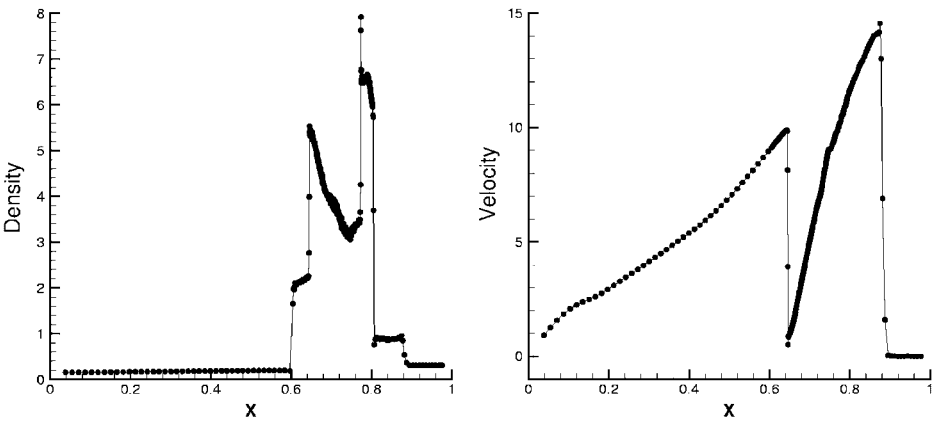

Figure 4. Blastwave—Density and velocity given by the 1D method for $m = 2$ with 400 cells. The line joins the average values between two adjadcent cells.

In Figure 4 density and velocity are presented for the present method (400 cells). In Figure 5 the density given by the Eulerian schemes for 400 cells is shown. The solution in a straight line is a converged solution given by the PPM scheme for 2000 cells.

Even if an overshoot can be observed for the present method, the results are very close to the converged solution. Shock waves and contact discontinuities are well solved.

For the 2D test case the results are presented with the particle method, the moments are projected on particles and then the particle population is drawn (a circle is drawn at the particle location and the colour represents the variable value). No interpolation has been made between the particle values to avoid visualization problems.

Isentropic compression of a ring in 2D planar geometry: The *Stiffened Gaz* equation of state $p_{SG} = p - \gamma\pi_\infty$ (p is the pressure from the perfect EOS, $\gamma = 3.5$, $\pi_\infty = 350 \times 10^9$) is

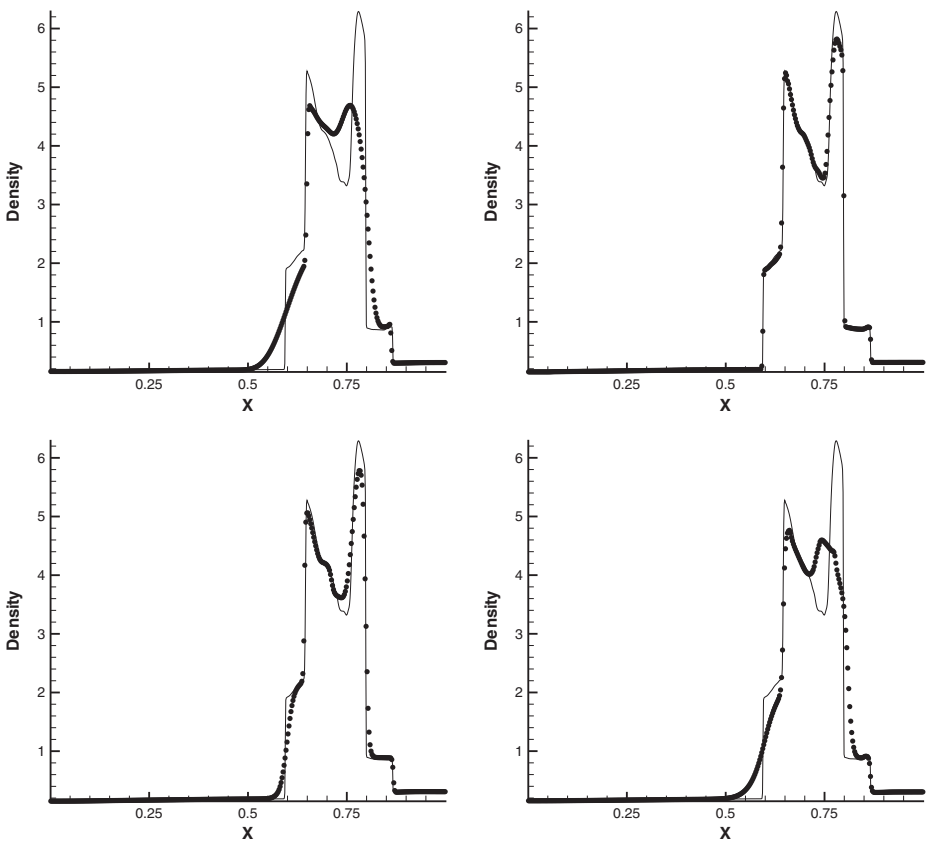

Figure 5. Blastwave—Density given by Eulerian methods with 400 cells. The straight line is the converged solution (2000 cells) given by the PPM method.

used. The initial density is $\rho = 7.82$, the initial pressure is $p_{SG} = 0$, the velocity is centripetal and $\|\overrightarrow{V}\| = 2 \times 10^5$. The radii of the ring are $R^+ = 10$ and $R^- = 9.5$, see Figure 6.

As vacuum is all around ($p_{ext} = 0$) there is no jump in pressure. Then the ring is moving towards its centre and at the same time is becoming thicker. Both phenomena should compensate each other and the average density of the ring should remain close to 7.82. Afterwards the compression will be much higher and the average density will increase until the ring closes on itself.

An unstructured mesh (51 points on circumferences of 11 concentrical circles, 2040 cells, 1071 mesh points) is used. The density on particles is presented for two times ($T_1 = 1.43 \times 10^{-6}$ and $T_2 = 38.8 \times 10^{-6}$) in Figure 7. The first difficulty of this test case is to retain the cylindricity of the problem, which seems to be achieved by this method for an unstructured mesh.

In Figure 8, the average density on the ring is shown for the present method and the 1D cylindrical Godunov scheme with 100 cells. Numerical oscillations for the two schemes are due to the fact that acoustic waves are generated due to the boundary conditions at the very

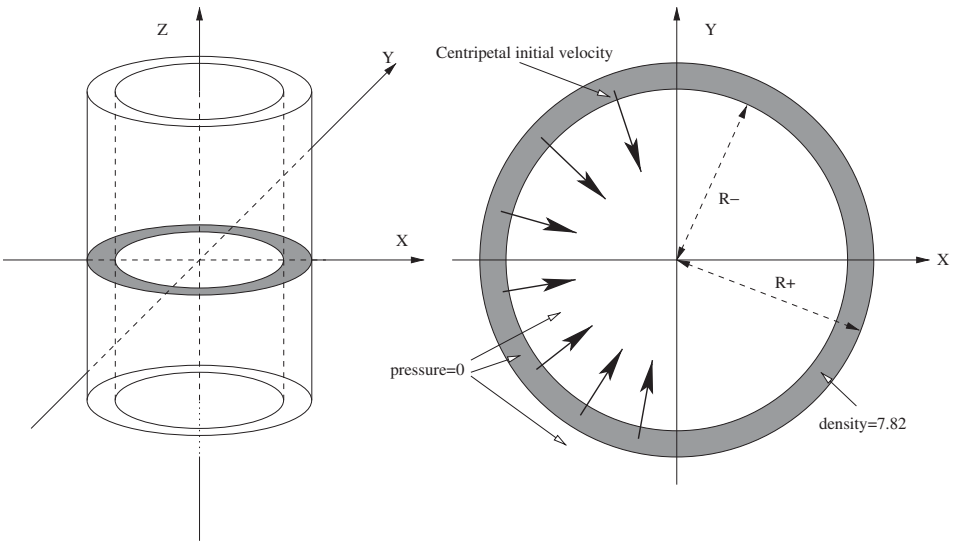

Figure 6. Isentropic compression of a ring—the ring is considered as a cut of an infinite cylinder (left) with a 2D cartesian geometry—sketch of the problem (right): the initial density is 7.82, the initial velocity is centripetal and $\|\vec{V}\| = 2 \times 10^5$, the pressure is zero inside and around the ring (the stiffened-gaz equation of state is used: $p_{SG} = p - \gamma\pi_\infty$ with p the pressure from the perfect EOS, $\gamma = 3.5$, $\pi_\infty = 350 \times 10^9$, the radii of the ring are $R^+ = 10$ and $R^- = 9.5$.

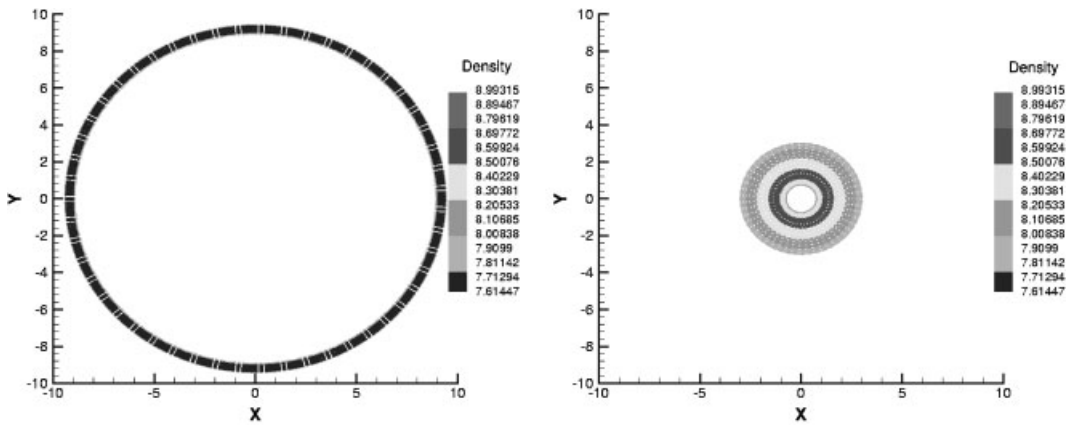

Figure 7. Isentropic compression of a ring—density on particles given by the 2D method for $m = 2$ at $T_1 = 1.43 \times 10^{-6}$ and $T_2 = 38.8 \times 10^{-6}$.

beginning of the computation. The second difficulty is to catch the right behaviour of the phenomenon, a first phase with a constant ring density, and a second phase where the ring density is increasing. The time of the transition between these phases seems to be well solved with this method even if the mesh is unstructured.

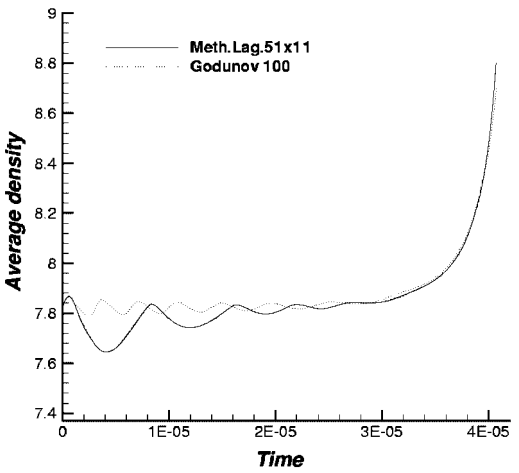

Figure 8. Isentropic compression of a ring—time evolution of the average density on the ring (present method and 1D cylindrical Godunov scheme with 100 cells).

7. CONCLUSION

In this paper, a new Lagrangian Discontinuous Galerkin-type method on unstructured meshes has been presented. A non-classical Lagrangian formulation of the Euler equations is solved. Using Bernstein polynomials we are able to define (m)-diffusive polynomials which add some numerical diffusion to the scheme during the computation of the increment terms. We show that this numerical diffusion is sufficient to ensure the conservation of the positivity. An acoustic Riemann solver is used to treat the discontinuity at the interfaces and a Runge–Kutta (or implicit) method is used for time discretization. Such a method defines a hierarchical class of numerical schemes depending on the degree of the Bernstein basis. The remeshing/remapping phase is treated with a particle method: this process is locally conservative and its accuracy can be adapted to the accuracy of the scheme. In 1D and 2D, some test cases show the efficiency of this method to treat shock waves, contact discontinuities, expansion waves or cylindrical phenomena without the need for remeshing/remapping. In particular the isentropic compressions can be treated with such a method on unstructured meshes without breaking the symmetry of the problem.

ACKNOWLEDGEMENTS

The first author thanks H. Jourdren (CEA-DIF) for fruitful discussions and for having suggested the isentropic compression test case. The authors thank R. Liska and B. Wendroff for their help to obtain the Eulerian results, and the referees for their comments and suggestions that resulted in an improved version of this paper.

REFERENCES

1. Hui WH, Li PY, Li ZW. A unified coordinate system for solving the two-dimensional Euler equations. *Journal of Computational Physics* 1999; **153**:596–637.

2. Hui WH, He Y. Hyperbolicity and optimal coordinates for the three-dimensional supersonic Euler equations. *SIAM Journal of Applied Mathematics* 1997; **57**:893–928.
3. Loubère R. A new Lagrangian Discontinuous Galerkin particle type method. Applications to hydrodynamics and laser/plasma interaction problems. *Ph.D. Thesis*, University of Bordeaux 2002 (in French).
4. Liska R, Wendroff B. Comparision of several difference schemes on 1D and 2D test problems for the Euler equations. *Conservation Laws Preprint Server*, http://www.math.ntnu.no/conservation/, 2001.
5. Loubère R, Ovadia J. A Lagrangian particle method. Part 1: principles of the method. *Technical Report LRC-M03*, CEA-Univ. Bordeaux 1, 2001 (in French).
6. Bonnaud G, Loubère R, Ovadia J. A Lagrangian particle method. Part 2: application to laser/plasma interaction problems. *Technical Report LRC-M03*, CEA-Univ. Bordeaux 1, 2001 (in French).
7. Guillard H, Abgrall R. *Modélisation Numérique des Fluides Compressibles*, Series in Applied Mathematics. Cialet PG, Lions PL (eds); North-Holland: Amsterdam, 2001.
8. Knupp PM. Algebraic mesh quality metrics. *SIAM Journal of Scientific Computing* 2001; **23**(1):198–218.

